JOURNAL OF SYNCHROTRON RADIATION
ISSN 1600-5775

Investigation of a CPG-array CdZnTe γ-ray imaging detector with single collecting electrodes readout

Yuedong Ma,* Shali Xiao, Guoqiang Yang and Liuqiang Zhang

Key Laboratory of Optoelectronic Technology and Systems, Ministry of Education, Chongqing University, Chongqing 400044, People's Republic of China. *Correspondence e-mail: mayuedong@cqu.edu.cn

Received 16 March 2015
Accepted 22 August 2015

Edited by A. Momose, Tohoku University, Japan

Keywords: coplanar grid; CdZnTe; charge induction efficiency; γ-ray detector; imaging; energy spectrum.

The single-electrode readout method has been applied to a coplanar grid (CPG) array CdZnTe detector in order to halve the number of preamplifiers previously needed and to facilitate imaging applications of CPG detectors. A method of predetermining the width of the optimum collecting electrodes has also been proposed, using the calculated optimum relative gain factor G. Meanwhile, a detailed process for calculating the charge induction efficiency (CIE) is presented. To simplify the calculation process, the computational formula of the CIE was deduced through the integration of the weighting potential. For performance evaluation, a 2×2 CPG-array CdZnTe detector was elaborately designed and tested with ^{137}Cs at 662 keV. Experimental results showed the capability of using the CPG-array CdZnTe detector with single collecting electrode readout for γ-ray imaging applications, with the same complexity of associated readout electronics as that of the pixelated CdZnTe detectors.

1. Introduction

The CdZnTe crystal is a promising candidate for hard X-ray and γ-ray detection owing to its attractive properties. Compared with other wide band-gap semiconductor materials, it shows advantages of high detection efficiency, good spectroscopic performance and room-temperature operation (Zhang *et al.*, 2013). Nevertheless, it also has shortcomings of serious holes trapping, leading to degradation of the measured energy spectrum. Therefore, various kinds of unipolarity CdZnTe detectors have been developed, such as the pixelated, strip, virtual Frisch, coplanar grid (CPG) and hemisphere detectors. A common characteristic of these unipolarity CdZnTe detectors is that their response is mainly due to the movement of electrons within the detectors.

As one of the unipolarity CdZnTe detectors, the CPG detector consists of two interdigitated electrodes on the anode surface. The response of the detector is acquired through subtracting the signals induced on the non-collecting grid (NCG) from that induced on the collecting grid (CG). In contrast to other unipolarity CdZnTe detectors, the charge induction efficiency (CIE) of the CPG detectors is highly uniform, intrinsically leading to a good spectral response (Luke, 1996). Another advantage of the CPG detectors is that the associated readout electronics are relatively simple. Consequently, CPG CdZnTe detectors are widely used as γ-ray spectrometers (Luke *et al.*, 2001, 2005; Prettyman *et al.*, 2001).

Besides detecting the energy spectrum, some imaging applications are also needed for γ-ray semiconductor detectors such as for positron emission tomography and single photon emission tomography (Gu *et al.*, 2011). However, CPG detectors are rarely used for γ-ray imaging applications,

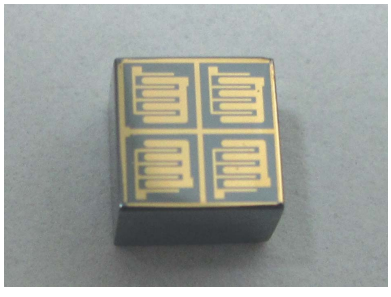

mainly for two reasons. Firstly, CPG detectors are generally used to detect the energy spectrum with one large CPG pair on the anode surface, hence with no spatial resolution. Secondly, the imaging application requires a large number of CPG pairs, resulting in extremely complex readout electronics. If the number of CPG pairs on the anode surface is N, the number of preamplifiers needed would be $2N$.

To provide CPG detectors with spatial discrimination, some efforts have been made with or without intention. Luke *et al.* (2001) developed four independent 1 cm^3 CPG detectors with attached readout electronics and assembled them together to form a 2×2 array for environmental remediation. He *et al.* (2005) employed four independent CPG electrode pairs on the anode and cathode surface of a 30 mm × 30.5 mm × 12 mm CdZnTe crystal to improve the detection efficiency. The obtained spatial resolutions of both detectors were approximately 14 mm. We have designed a CPG-array CdZnTe detector, consisting of a 2×2 CPG pairs array on the anode surface of a 7 mm × 7 mm × 5 mm CdZnTe crystal. The obtained intrinsic spatial resolution was 3.3 mm and the energy resolution at 662 keV was 2.7% (Ma *et al.*, 2014).

We have proved previously that CPG CdZnTe detectors could have a much better spatial resolution but still with a good energy resolution. Hence, if the readout electronics could be greatly simplified, CPG detectors could be potentially applied for some γ-ray imaging applications. For a CPG detector with a single CPG pair on the anode surface, Amman & Luke (1997) have shown that, by properly adjusting the width of the collecting electrodes and non-collecting electrodes, the response of the detector can be obtained by reading out the signals from the collecting grid.

In this paper, to explore the possibility of using the CPG CdZnTe detector as an imaging tool, we utilized the single-electrode readout method in a 2×2 CPG-array CdZnTe detector in order to halve the number of total preamplifiers needed previously. This paper is structured as follows. In §2, the single-electrode readout method is discussed further. The optimum width of the collecting electrodes (w_c) and the non-collecting electrodes (w_{nc}) was predetermined. Meanwhile, to simplify the calculation of the CIE distribution, we also deduced the computational formula of the CIE for the CPG detectors through the integration of the weighting potential. Following that, in §3, the design of the CPG-array CdZnTe detector with dimensions of 7 mm × 7 mm × 5 mm is given. The spectroscopic performance of the detector is also presented.

2. Further discussion on single-electrode readout

2.1. The single-electrode readout method

The relative gain method is always adopted by CPG detectors to compensate for electron trapping by subtracting only a fraction of the signals collected by the NCG. However, essentially, the single-electrode readout method can be regarded as another way of compensating for electron trapping for the CPG detectors. Electron trapping occurs within the detector when the electrons created by energy deposition drift to the collecting electrodes. Since the electrons attenuate exponentially with drifting distance, the electrons created near the cathode surface will be trapped more seriously compared with those created near the anode surface. As a result, the spectral response of the detector will be degraded with variation of the interaction depth.

The relative gain method is suitable for CPG detectors with the same w_c and w_{nc}. The best spectral response will be obtained when the optimum relative gain factor G is adopted. At this time, if we regard the weighting potential of the CG and NCG as Φ_{CG} and Φ_{NCG}, respectively, the CIE distribution calculated by $\Phi_{CG} - G\Phi_{NCG}$ is the flattest, which implies that the detector response is not depth-dependent, *i.e.* the trapped electrons are well compensated.

However, by applying the single-electrode readout method, w_c and w_{nc} of the CPG detectors will be different. Compensation of electron trapping is accomplished by varying Φ_{CG} and reading out the signals from only the CG. Actually, Φ_{CG} will be changed with w_c and w_{nc}. Fig. 1 shows different Φ_{CG} values of two 6.12 mm × 6.12 mm × 5 mm CPG CdZnTe detectors (D_1 and D_2). Both of the detectors have a pitch and gap (the distance between the collecting electrode and the neighboring non-collecting electrode) of 1 mm and 0.12 mm, respectively. The difference is that D_1 has the same w_c and w_{nc} of 0.38 mm, while w_c and w_{nc} of D_2 are 0.10 mm and 0.66 mm, respectively. After decreasing w_c and increasing w_{nc} while keeping the pitch and gap constant, the slope of Φ_{CG} in the far-grid region becomes much slower (see Fig. 1*b*). As a result, the induced charges on the CG by the movement of the electrons in the far-grid region are decreased. If we regard the CIE distribution calculated by Φ_{CG} as CIE_{cg}, likewise, the CIE distributions calculated by $\Phi_{CG} - G\Phi_{NCG}$ will be regarded as $CIE_{cg\text{-}Gncg}$. Assuming that the two detectors have the same mobility-lifetime products and applied bias, by properly adjusting w_c and w_{nc} of D_2 the electron trapping within D_2 will also be well compensated once CIE_{cg} of D_2 is almost the same as $CIE_{cg\text{-}Gncg}$ of D_1.

Given that the current w_c and w_{nc} may not be optimal for D_2, applying the single-electrode readout method to D_2 includes two steps. The first step is to determine the optimum relative gain coefficient G of D_1 by finding out the flattest $CIE_{cg\text{-}Gncg}$ of D_1. The calculated $CIE_{cg\text{-}Gncg}$ for different G is presented in Fig. 2(*a*), assuming $\mu_e\tau_e = 3 \times 10^{-3}$ $cm^2\,V^{-1}$, $\mu_h\tau_h = 2 \times 10^{-4}$ $cm^2\,V^{-1}$ and the applied bias $V_b = 500$ V. Since the CIE distribution is flattest when G is 0.6, the optimum value of G for D_1 is 0.6.

The second step is to determine the optimum w_c and w_{nc} of D_2 by finding the CIE_{cg} of D_2 that is most similar to $CIE_{cg\text{-}0.6ncg}$ of D_1. Fig. 2(*b*) shows the weighting potentials Φ_{CG} of D_2 for different w_c, as well as $\Phi_{CG} - 0.6\Phi_{NCG}$ of D_1. Accordingly, Fig. 2(*c*) draws a different CIE curve corresponding to the weighting potentials shown in Fig. 2(*b*). It shows that when w_c of D_2 is 0.08 mm, Φ_{CG} of D_2 is similar to $\Phi_{CG} - 0.6\Phi_{NCG}$ of D_1, leading to the similar CIE_{cg} of D_2 and $CIE_{cg\text{-}0.6ncg}$ of D_1, especially in the far-grid region. Therefore, the optimum w_c of D_2 is 0.08 mm.

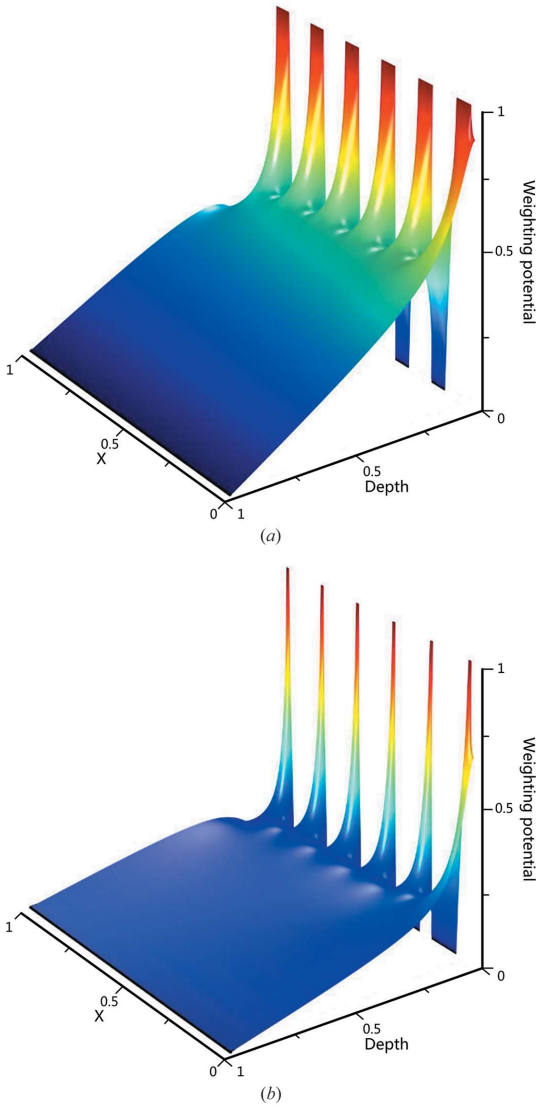

Figure 1
Weighting potentials of the collecting grid (Φ_{CG}) of two 6.12 mm × 6.12 mm × 5 mm CPG CdZnTe detectors (D_1 and D_2) with the same pitch and gap of 1 mm and 0.12 mm, respectively. All three axes have been normalized. (*a*) Φ_{CG} of D_1. w_c and w_{nc} are both 0.38 mm. (*b*) Φ_{CG} of D_2. w_c and w_{nc} are 0.10 mm and 0.66 mm, respectively.

2.2. Predetermination of the optimum w_c

As mentioned above, using the single-electrode readout method not only simplifies the readout electronics but also compensates the electron trapping effect within the detector. However, it seems quite complicated to apply this method. Before the optimum w_c can be decided a series of calculations of the weighting potentials and CIE distributions are still needed with optimum G determined. To simplify the determination of w_c, so as to facilitate the application of the single-electrode readout method, we present a new way to predetermine the optimum w_c based on the induced relationship between w_c and the optimum G.

In this section we first look into the relationship between the optimum w_c of D_2 and the optimum G of D_1, and demonstrate the relevance. Since Φ_{CG} of D_2 with optimum w_c is identical to $\Phi_{CG} - G\Phi_{NCG}$ of D_1 with optimum G in the far-grid region, as shown in Fig. 2(*b*), the responses of D_1 and D_2 stimulated by the γ-rays with the same photon energy which interact at the same position should also be identical when the

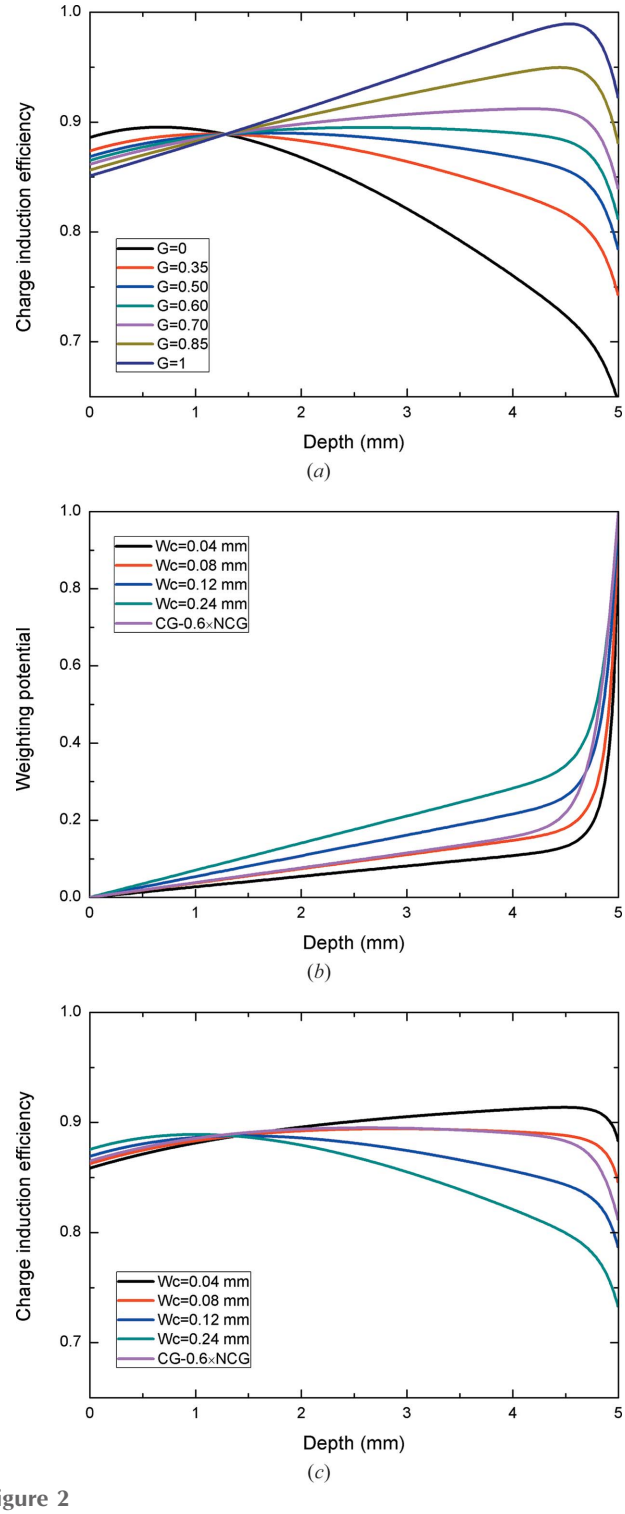

Figure 2
(*a*) Calculated $CIE_{cg\text{-}Gncg}$ under different relative gain coefficient G, assuming $\mu_e\tau_e = 3 \times 10^{-3}$ cm^2 V^{-1}, $\mu_h\tau_h = 2 \times 10^{-4}$ cm^2 V^{-1} and the applied bias $V_b = 500$ V. (*b*) $\Phi_{CG} - 0.6\Phi_{NCG}$ of D_1 as well as Φ_{CG} of D_2 under different w_c. (*c*) CIE curves corresponding to the weighting potentials shown in (*b*).

generated electrons drift in the far-grid region (here we ignore the difference of the local material properties and assume that the interactions of the γ-rays and the material are all by the photoelectric effect).

Owing to the pitch, gap and strip numbers of the two detectors being the same, the effective overlap area between the cathode and all the collecting and non-collecting electrodes on the anode surface of the two detectors are also the same. Since the total capacity $C_{\rm tot}$ from the interaction point to all the electrodes in the anode surface is proportional to the effective overlap area, $C_{\rm tot}$ for the two detectors are identical. According to the static charge analysis and capacitance coupling method (Lingren & Butler, 1998), the totally induced transient charge on the electrodes by the γ-rays is proportional to $C_{\rm tot}$. Therefore, the induced transient charge on the electrodes on the anode surface of D_1 and D_2 are also the same.

Suppose that the induced transient charge on CG and NCG of D_1 and D_2 by the γ-rays is Q. For detector D_1 the induced charge on CG and NCG will be $Q/2$. After subtracting the induced charge on NCG, the instantaneous response R_1 of D_1 will be

$$R_1 = \frac{Q}{2}(1 - G). \tag{1}$$

If we assume that the distribution of the weighting potential changes linearly between collecting electrodes and non-collecting electrodes on the anode surface, then for the generated charges drifting in the far-grid region the induced charges on the collecting electrodes of D_2 (Amman & Luke, 1997), *i.e.* the instantaneous response R_2 of D_2, is approximately

$$R_2 = \frac{w_{\rm c} + g}{p}\, Q, \tag{2}$$

where g is the gap, p is the pitch ($p = w_{\rm c} + w_{\rm nc} + 2g$).

As mentioned above, R_2 should be equal to R_1. Therefore, by combining (1) and (2) we have

$$\frac{Q}{2}(1 - G) = \frac{w_{\rm c} + g}{p}\, Q. \tag{3}$$

Using (3), the optimum $w_{\rm c}$ and $w_{\rm nc}$ can be given as

$$w_{\rm c} = \frac{p}{2}(1 - G) - g, \qquad w_{\rm nc} = \frac{p}{2}(1 + G) - g. \tag{4}$$

Hence, the optimum $w_{\rm c}$ can be predetermined by the optimum G.

To demonstrate equation (4), we first determined the optimum $w_{\rm c}$ of D_2 under different biases. By assuming $\mu_{\rm e}\tau_{\rm e} = 3 \times 10^{-3}$ cm^2 V^{-1}, $\mu_{\rm h}\tau_{\rm h} = 2 \times 10^{-4}$ cm^2 V^{-1}, the flattest $\mathrm{CIE}_{\mathrm{cg}\text{-}G\mathrm{ncg}}$ of D_2 under the applied bias of 150 V, 300 V, 450 V and 600 V, respectively, are found. The optimum G of 0.25, 0.45, 0.55 and 0.60 are determined accordingly. Subsequently, from (4), the optimum $w_{\rm c}$ under the different biases are 0.255 mm, 0.155 mm, 0.105 mm and 0.080 mm, respectively. Finally, for the different biases, $\mathrm{CIE}_{\mathrm{cg}\text{-}G\mathrm{ncg}}$ under the optimum G are compared with the corresponding $\mathrm{CIE}_{\rm cg}$ under the optimum $w_{\rm c}$, as shown in Fig. 3. Since the CIE curves fit very well with each other, especially in the far-grid region, equation (4) is verified. The differences of the CIE curves in the near-grid region are due to equation (2) only being suitable for use in the far-grid region.

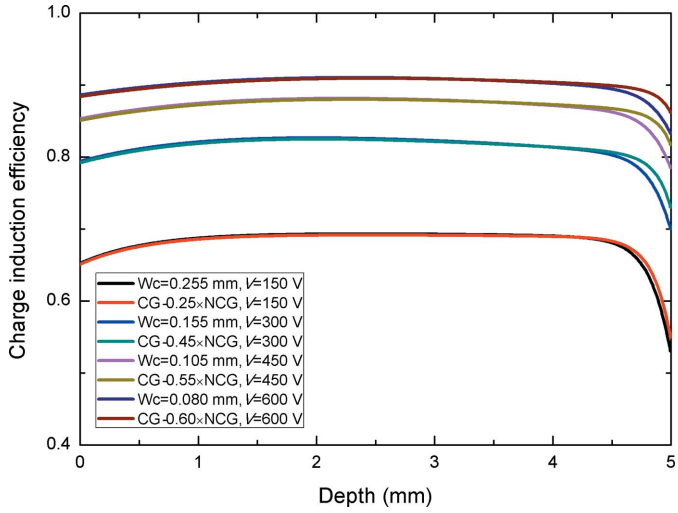

Figure 3
Comparison of $\mathrm{CIE}_{\rm cg}$ of D_2 and $\mathrm{CIE}_{\mathrm{cg}\text{-}G\mathrm{ncg}}$ of D_1under the optimum $w_{\rm c}$ and the corresponding optimum G, for biases of 150 V, 300 V, 450 V and 600 V. Mobility-lifetime products of the two detectors are assumed to be $\mu_{\rm e}\tau_{\rm e} = 3 \times 10^{-3}$ cm^2 V^{-1}, $\mu_{\rm h}\tau_h = 2 \times 10^{-4}$ cm^2 V^{-1}.

2.3. Charge induction efficiency of CPG CdZnTe detectors

The CIE distribution indicates the uniformity of the detector response. Furthermore, the application of the single-electrode readout method involves calculation and comparison of a series of CIE curves under different mobility-lifetime products and applied biases. Therefore, it is important to find an easy approach to obtaining the CIE distribution. Odaka *et al.* (2010) have proposed a method of calculating the CIE through the integration of the weighting field. In this paper, a detailed calculation process of the CIE was presented. To simplify the calculation process, we deduced the computational formula of the CIE through the integration of the weighting potential.

The charge induction efficiency at a given point r_0 within the detector is defined as

$$\mathrm{CIE}(r_0) = \frac{Q_{\mathrm{tot\_in}}(r_0)}{Q_0}, \tag{5}$$

where Q_0 is the charge originally created by the energy deposition at the interaction point r_0, and $Q_{\mathrm{tot\_in}}(r_0)$ is the total induced charge on the electrodes resulting from the movement of Q_0.

It is worth mentioning that charge trapping occurs when Q_0 is moving in the detector. Assuming that, after drifting from r_0, r_1, r_2,... to r_i, Q_0 becomes $Q(r_i)$. By applying the Shockley–Ramo theorem (Shockley, 1938; Ramo, 1939), the induced transient charge $Q_{\rm in}(r_i)$ by the movement of $Q(r_i)$ can be given as

$$\Delta Q_{\rm in}(r_i) = Q(r_i)\mathbf{E}_{\rm w}(r_i)\Delta\mathbf{r}_i = Q(r_i)\Delta\Phi(r_i), \tag{6}$$

where $\mathbf{E}_w(r_i)$ and $\Phi(r_i)$ are the weighting field and weighting potential at point r_i, respectively. Assuming that, in very short time Δt, the charges drift from r_i to r_{i+1}, then $\Delta\mathbf{r}_i = \mathbf{r}_{i+1} - \mathbf{r}_i$, where $\mathbf{r}_i$ and $\mathbf{r}_{i+1}$ are the vectors pointing from the original point in space to r_i and r_{i-1}, respectively.

$Q(r_i)$ and Q_0 can be related by

$$Q_{e,h}(r) = Q_0 \exp\left[-\left(\sum_{j=0}^{i-1}|\Delta\mathbf{r}_j|\right)/\lambda_{e,h}\right], \tag{7}$$

where λ_e and λ_h are the mean free drift length of electrons and holes ($\lambda_e = \mu_e\tau_e E$, $\lambda_h = \mu_h\tau_h E$), and $|\Delta\mathbf{r}_j|$ is the norm of vector $\Delta\mathbf{r}_j$. Assuming that the electrons drift from r_k to r_{k+1}, $r_{k+2}, \ldots, r_n$, and finally reach the collecting electrodes, likewise, the holes drift from r_k to r_{k-1}, $r_{k-2} \ldots r_0$, and reach the cathode (see Fig. 4). Combining (6) and (7), the total induced charges $Q_{\text{tot\_in}}(r_0)$ can be written as

$$\begin{aligned} Q_{\text{tot\_in}}(r_k) &= Q_{\text{tot\_in e}}(r_k) + Q_{\text{tot\_in h}}(r_k) \\ &= \sum_{i=k+1}^{n} Q_e(r_i)\Delta\Phi(r_i) + \sum_{i=1}^{k} Q_h(r_i)\Delta\Phi(r_i) \\ &= Q_0\left[\Phi(r_i) - \Phi(r_{i-1})\right] \\ &\quad \times \left\{\sum_{i=k+1}^{n} \exp\left[-\left(\sum_{j=k}^{i-1}|\Delta\mathbf{r}_j|\right)/\lambda_e\right]\right. \\ &\quad \left. + \sum_{i=1}^{k} \exp\left[-\left(\sum_{j=k-1}^{i-1}|\Delta\mathbf{r}_j|\right)/\lambda_h\right]\right\}, \end{aligned} \tag{8}$$

where $Q_{\text{tot\_in e}}(r_0)$ and $Q_{\text{tot\_in h}}(r_0)$ are the total induced charges contributed from electrons and holes, respectively. From (8) and (5), $\text{CIE}(r_k)$ can be rewritten as

$$\begin{aligned} \text{CIE}(r_k) = \left[\Phi(r_i) - \Phi(r_{i-1})\right]&\left\{\sum_{i=k+1}^{n} \exp\left[-\left(\sum_{j=k}^{i-1}|\Delta\mathbf{r}_j|\right)/\lambda_e\right]\right. \\ &\left. + \sum_{i=1}^{k} \exp\left[-\left(\sum_{j=k-1}^{i-1}|\Delta\mathbf{r}_j|\right)/\lambda_h\right]\right\}. \end{aligned} \tag{9}$$

Because $\mathbf{r}$ is a three-dimensional space vector, the calculation of CIE is rather complicated. To simplify the calculation, we assume that the γ-ray is deposited on a point of the central line of one collecting electrode x_k. Then the created electron–hole pairs will drift along the central line. If we equally divide the depth of the detector into n parts (n is large enough), from cathode surface x_0 to anode surface x_n, equation (9) can be simplified to

$$\begin{aligned} \text{CIE}(x_k) = \left[\Phi(x_i) - \Phi(x_{i-1})\right]&\left[\sum_{i=1}^{k} \exp\left(-\frac{x_k - x_i}{\lambda_h}\right)\right. \\ &\left. + \sum_{i=k+1}^{n} \exp\left(-\frac{x_i - x_k}{\lambda_e}\right)\right]. \end{aligned} \tag{10}$$

Equation (10) can also be used for planar CdZnTe detectors. If the depth of the detector is L, then $\Phi_w(x) = x/L$. Hence equation (10) can be converted to integral form,

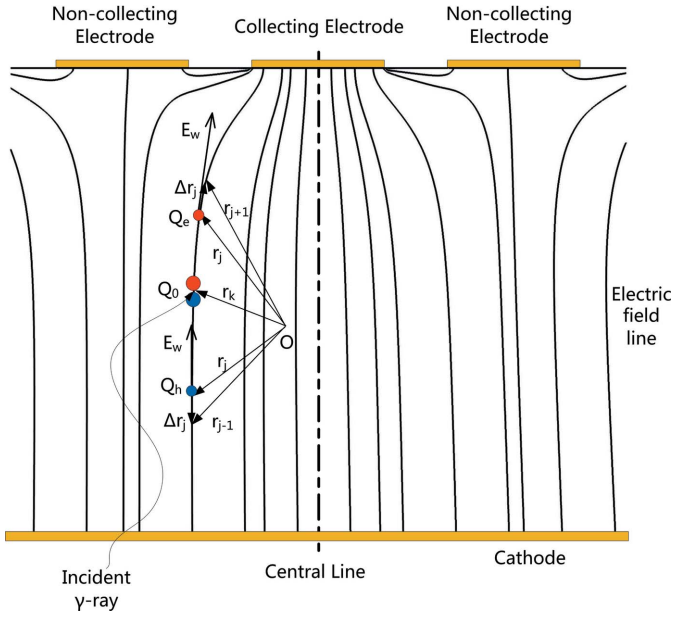

Figure 4
Schematic diagram of charges drifting in the CPG CdZnTe detectors. Q_0 is created by γ-ray deposition at the interaction point r_k. Then the electrons drift along the electric field line, from point r_k to $r_{k+1}, r_{k+2}, \ldots, r_n$, and finally reach the collecting electrodes; likewise, the holes drift from r_k to $r_{k-1}, r_{k-2}, \ldots, r_0$, and reach the cathode. O is the original point in space. $\mathbf{r}_j$ is the vector from O to the point r_j on the electric field line. For the electrons, $j = k, k+1, \ldots, n$, while, for the holes, $j = 0, 1, \ldots, k$. The relationship between Q_e, Q_h and Q_0 is shown in equation (7). The charges totally induced on the collecting electrodes by the movement of Q_0 can be obtained by equation (8).

$$\begin{aligned} \text{CIE}(x_k) &= \int_{x_k}^{0} \exp\left(-\frac{x_k - x}{\lambda_h}\right) \mathrm{d}\Phi(x) \\ &\quad + \int_{x_k}^{L} \exp\left(-\frac{x - x_k}{\lambda_e}\right) \mathrm{d}\Phi(x) \\ &= \frac{\lambda_h}{L}\left[1 - \exp\left(-\frac{x_k}{\lambda_h}\right)\right] + \frac{\lambda_e}{L}\left[1 - \exp\left(-\frac{L - x_k}{\lambda_e}\right)\right]. \end{aligned} \tag{11}$$

As a result, equation (11) is identical to the Hecht equation (Akutagawa & Zanio, 1969).

3. Experimental results

3.1. Design of the CPG-array CdZnTe detector

We applied the single-electrode readout method to a 2 × 2 CPG-array CdZnTe detector. The CdZnTe detector used in this work was grown by the modified vertical Bridgman method. A number of crystals with the same dimensions were first made into planar detectors. Only the detector with the best energy spectrum of alpha particles was selected. The measured electron and hole mobility-lifetime products of the selected crystal are $\mu_e\tau_e = 2.4 \times 10^{-3}$ cm^2 V^{-1} and $\mu_h\tau_h = 2 \times 10^{-4}$ cm^2 V^{-1}. With a bias of 300 V, the optimum G was determined to be 0.33, with the flattest $\text{CIE}_{\text{cg-}G\text{ncg}}$ found, as shown in Fig. 5.

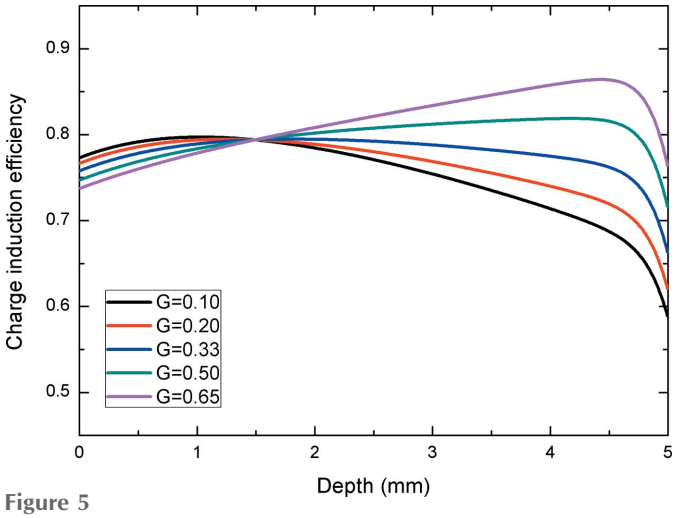

Figure 5
$CIE_{cg\text{-}Gncg}$ under different relative gain coefficient G, for a bias voltage of 300 V. The CIE curve is flattest when $G = 0.33$; therefore the optimum G is 0.33.

Note that the choice of the applied bias is also crucial. A larger bias over a detector always leads to a better spectral performance as well as a smaller optimum w_c (Amman & Luke, 1997). However, w_c cannot be too small, because of the charge loss on the surface between the strips, which is similar to that occurring in the pixellated detectors (Bolotnikov *et al.*, 1999). Charge loss on the surface occurs because the surface of the CdZnTe crystal is not an ideal dielectric, so the electric field lines will partly terminate on the surface between the strips. When w_c is extremely small, especially much smaller than the radius of the electron clouds which approach the anode surface, charge loss will be evident and a lot of charges would be trapped on the surface. Therefore, when determining the optimum bias, attention should be paid to the prevention of serious degradation of the detection efficiency caused by the extremely small w_c. Accordingly, in this paper the optimum bias was set to 300 V, and the corresponding optimum w_c was determined to be 0.1 mm, based on equation (4).

Fig. 6 shows the anode surface of the designed CPG-array CdZnTe detector with dimensions of 7 mm × 7 mm × 5 mm. The cathode surface of the detector is a planar electrode. Four identical CPG pairs (P_{11}, P_{12}, P_{21} and P_{22}) are presented on the anode surface, forming a 2 × 2 array, which are separated and surrounded by the boundary electrode. Each of the CPG pairs consists of four interdigitated collecting strips and non-collecting strips. The pitch and gap of the detector are 0.6 mm and 0.1 mm, respectively. As mentioned above, the optimum w_c was determined to be 0.1 mm, according to equation (4). Accordingly, w_{nc} was determined to be 0.3 mm. The intrinsic spatial resolution of the detector is 3.3 mm, which implies that the detector can be applied to some γ-ray imaging applications.

3.2. Spectroscopic performance

The spectroscopic performance of the CPG-array CdZnTe detector was measured with ^{137}Cs at 662 keV at room temperature. The detector was first placed in a shielding box to avoid electromagnetic interference. The cathode and non-collecting electrodes were set to −300 V and −30 V, respectively. The collecting electrodes and the boundary electrode were both set to ground. To maintain the symmetry of the weighting potential when operated, all the CPG pairs were biased in the same situation as mentioned above. The four CPG pairs were then tested one after another. The signals on the collecting electrodes of each CPG pair were read out by a charge-sensitive preamplifier and a shaping amplifier. Eventually the pulse-height spectra were obtained by a digital multi-channel analyzer.

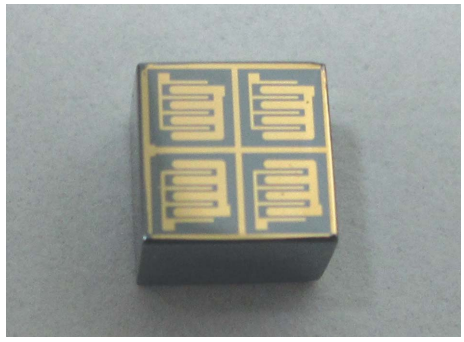

Figure 6
The anode surface of the 2 × 2 CPG-array CdZnTe detector that we designed, with dimensions of 7 mm × 7 mm × 5 mm.

Fig. 7 shows the obtained energy spectra of ^{137}Cs at 662 keV with the tested CPG-array CdZnTe detector. The energy resolutions of the four CPG pairs are 3.7%, 4.1%, 4.4% and 4.7%, respectively. The variation of the energy resolutions from the identical CPG pairs may result from the local difference of the material properties of the CdZnTe crystals. Meanwhile, peak-to-Compton ratio (p/c) and peak-to-valley ratio (p/v) for all the CPG pairs are also shown in Fig. 7. Interestingly, CPG pairs with better spectral performance tend to have better p/c and p/v.

4. Conclusions

In this paper we applied the single-electrode readout method to a 2 × 2 CPG-array CdZnTe detector, hoping to facilitate the imaging application of CPG detectors. With this method the number of all preamplifiers was halved. The optimum w_c was also predetermined using the optimum relative gain factor G for a given charge mobility-lifetime product and applied bias. Meanwhile, a detailed process for calculating the CIE was presented. To simplify the calculation process, the computational formula for the CIE was deduced through the integration of the weighting potential. A CPG-array CdZnTe detector was designed based on the derivations and the tested energy resolution of ^{137}Cs at 662 keV was 3.7–4.7%. The results demonstrate that the CPG-array CdZnTe detector with single collecting electrode readout can be applied for γ-ray imaging application, with the same complexity of associated readout electronics as that of the pixelated CdZnTe detectors.

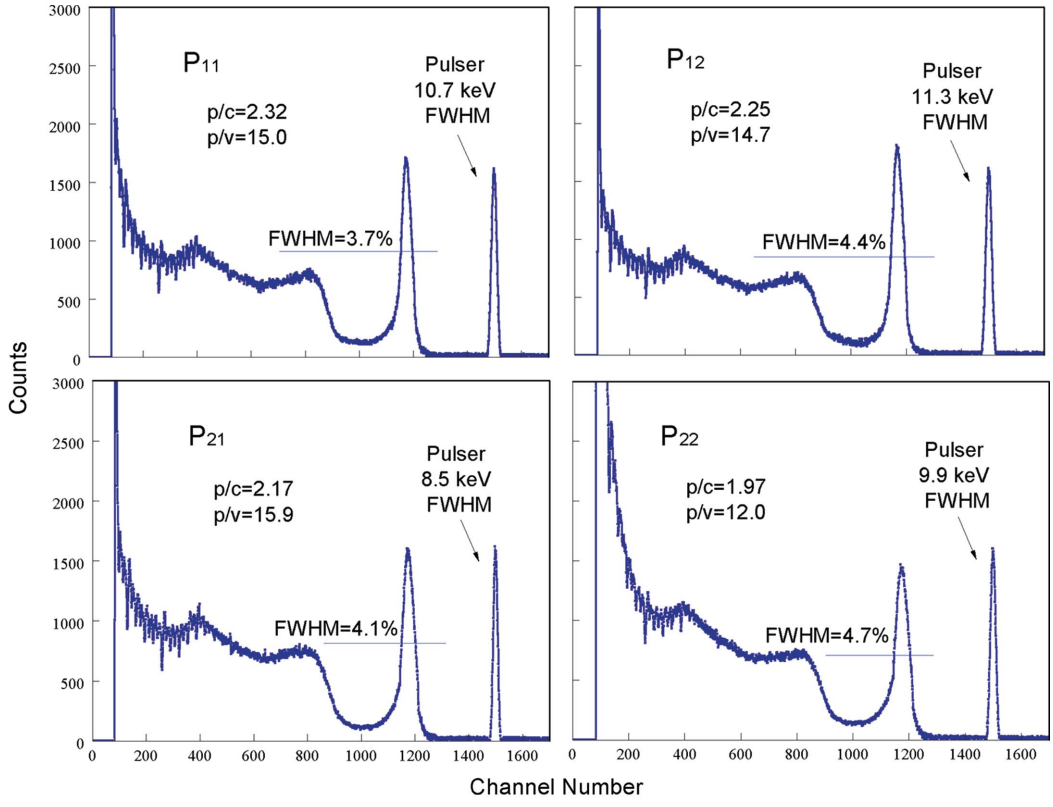

Figure 7
Energy spectra of ^{137}Cs at 662 keV of the CPG-array CdZnTe detector.

Acknowledgements

This work is supported by the National Natural Science Foundation of China (No. 61274048).

References

Akutagawa, W. & Zanio, K. (1969). *J. Appl. Phys.* **40**, 3838–3854.
Amman, M. & Luke, P. N. (1997). *Proc. SPIE*, **3115**, 205–213.
Bolotnikov, A. E., Cook, W. R., Harrison, F. A., Wong, A. S., Schindler, S. M. & Eichelberger, A. C. (1999). *Nucl. Instrum. Methods Phys. Res. A*, **432**, 326–331.
Gu, Y., Matteson, J. L., Skelton, R. T., Deal, A. C., Stephan, E. A., Duttweiler, F., Gasaway, T. M. & Levin, C. S. (2011). *Phys. Med. Biol.* **56**, 1563–1584.
He, Z., Sturm, B. W. & Rhodes, E. (2005). *Nucl. Sci. Symp. Conf. Rec. 2005 IEEE*, pp. 1159–1162.
Lingren, C. L. & Butler, J. F. (1998). *IEEE Trans. Nucl. Sci.* **45**, 1723–1725.
Luke, P. N. (1996). *Nucl. Instrum. Methods Phys. Res. A*, **380**, 232–237.
Luke, P. N., Amman, M., Lee, J. S., Ludewigt, B. A. & Yaver, H. (2001). *Nucl. Instrum. Methods Phys. Res. A*, **458**, 319–324.
Luke, P. N., Amman, M., Lee, J. S. & Vu, C. Q. (2005). *IEEE Trans. Nucl. Sci.* **52**, 2041–2044.
Ma, Y., Xiao, S., Yang, G. & Zhang, L. (2014). *Appl. Radiat. Isot.* **94**, 314–318.
Odaka, H., Sugimoto, S., Ishikawa, S., Katsuta, J., Koseki, Y., Fukuyama, T., Saito, S., Sato, R., Sato, R., Watanabe, S., Kokubun, M., Takahashi, T., Takeda, S., Fukazawa, Y., Tanaka, T. & Tajima, H. (2010). *Nucl. Instrum. Methods Phys. Res. A*, **624**, 303–309.
Prettyman, T. H., Feldman, W. C., Fuller, K. R., Storms, S. A., Soldner, S. A., Szeles, C., Ameduri, F. P., Lawrence, D. J., Brown, M. C. & Moss, C. E. (2001). *Nucl. Sci. Symp. Conf. Rec. 2001 IEEE*, **61**, 63–67.
Ramo, S. (1939). *Proc. IRE*, **27**, 584–585.
Shockley, W. (1938). *J. Appl. Phys.* **9**, 635–636.
Zhang, Q., Zhang, C., Lu, Y., Yang, K. & Ren, Q. (2013). *Sensors*, **13**, 2447–2474.